

Continuum limit of lattice quasielectron wavefunctions

Aniket Patra¹, Birgit Hillebrecht¹, and Anne E B Nielsen^{1,2}

¹ Max-Planck-Institut für Physik komplexer Systeme, D-01187 Dresden, Germany

² Department of Physics and Astronomy, Aarhus University, Ny Munkegade 120, DK-8000 Aarhus C, Denmark

Abstract.

Trial states describing anyonic quasiholes in the Laughlin state were found early on, and it is therefore natural to expect that one should also be able to create anyonic quasielectrons. Nevertheless, the existing trial wavefunctions for quasielectrons show behaviors that are not compatible with the expected topological properties or their construction involves ad hoc elements. It was shown, however, that for lattice fractional quantum Hall systems, it is possible to find a relatively simple quasielectron wavefunction that has all the expected properties [New J. Phys. **20**, 033029 (2018)]. This naturally poses the question: what happens to this wavefunction in the continuum limit? Here we demonstrate that, although one obtains a finite continuum wavefunction when the quasielectron is on top of a lattice site, such a limit of the lattice quasielectron does not exist in general. In particular, if the quasielectron is put anywhere else than on a lattice site, the lattice wavefunction diverges when the continuum limit is approached. The divergence can be removed by projecting the state on the lowest Landau level, but we find that the projected state does also not have the properties expected for anyonic quasielectrons. We hence conclude that the lattice quasielectron wavefunction does not solve the difficulty of finding trial states for anyonic quasielectrons in the continuum.

Keywords: fractional QHE, fractional statistics, Monte Carlo simulations.

1. Introduction

The discovery of the fractional quantum Hall effect (FQHE) in heterojunctions in solids [1] marks the genesis of the enduring interest in strongly correlated topologically ordered systems [2–4]. The topology in the FQHE is manifested in the presence of quasiholes and quasielectrons, which are anyonic excitations with positive and negative charge, respectively. In such solid-state systems [1], similar experimental manipulations – increasing or decreasing the external magnetic field – lead to realizations of quasiholes or quasielectrons, respectively.

Kitaev pointed out the usefulness of anyons in fault-tolerant topological quantum computing [5]. The first step in achieving this, by utilizing the anyonic excitations appearing in the FQHE, is to theoretically understand them. The dimension of such systems' Hilbert space being exponential in the number of electrons renders it difficult

for obtaining numerical results *ab initio*. Descriptions in terms of ansatz wavefunctions have traditionally provided the way forward.

For example, Laughlin provided an ansatz wavefunction explaining the FQHE ground state at $1/3$ filling [6]. In the same paper, he also provided an ansatz for the quasihole excitation, where the electron density is locally decreased, by modifying the ground state wavefunction. However, the difficulty of obtaining an ansatz for the quasielectron, where the electron density at the location of the quasielectron needs to be increased, was immediately understood. This leads to a pole singularity due to the Pauli exclusion principle.

Distinct wavefunctions for quasiholes and quasielectrons in the FQHE with different filling fractions were introduced using several different approaches [6–9, 11–17]. Laughlin, in his paper, introduced an ansatz in terms of derivative operators $\partial/\partial Z_i$, where Z_i are the electron coordinates [6]. Under the composite fermion framework, Jeon and Jain proposed a different ansatz that has lower variational energy compared to the Laughlin ansatz [8]. This quasielectron ansatz can be thought of as a composite of a quasiparticle of negative charge $-2/3$ and a quasihole of charge $1/3$, orbiting around the common center of mass with positive relative angular momentum [9]. The subtleties of the braiding properties of similar wavefunctions for composite fermion quasiparticles were analyzed [10]. One can obtain a quasielectron wavefunction by using a physical clustering condition, where it must vanish when certain patterns of clusters of electrons are formed [11]. Another way to obtain quasielectron and quasihole ansätze is to consider correlation functions of certain rational CFTs that involve nonlocal operators [12–14]. How to construct all states in the Abelian quantum Hall hierarchy using the above quasihole and quasielectron wavefunctions was also explained [15]. An operator formalism describing the Laughlin quasielectron in FQH systems with periodic boundary conditions (i.e., on a 2-torus) is also known [16]. In all these descriptions, however, one observes that either the braiding statistics or the positions of the quasielectrons are not as expected for anyonic quasielectrons. A description in which all properties are as expected for anyonic quasielectrons was found in [17], but it required some *ad hoc* modifications of the trial states to obtain this result.

It is possible to write trial wavefunctions for quasiholes and quasielectrons on a lattice [18], which have a natural construction and all the expected topological properties. This description is particularly simple because the quasiparticle operators are written in terms of a single screened chiral boson field, and the density profiles are undistorted due to absence of additional screening requirements. Interesting strongly correlated topological phases such as topological Chern insulators are only present in such lattice systems [19–21]. These are, e.g., relevant for implementations in optical lattices. In this paper, we investigate the continuum limit of these lattice wavefunctions. This analysis of the continuum limit – necessary for the description of solid-state anyonic excitations – was absent in Ref. [18]. Although placing the quasielectron on a lattice site produces a finite trial wavefunction, our analytical calculations show that the continuum limit of the quasielectron does not exist in general. Additionally, we

show that an attempt to cure the wavefunction of this problem by projecting it on the lowest Landau level (LLL) in the continuum limit, as was alluded to in [6], does also not give a suitable trial state for anyonic quasielectrons. In particular, the LLL-projected continuum quasielectron ansatz does not have the expected braiding properties.

We recapitulate the Laughlin wavefunctions for the continuum FQH ground state and the quasihole in Section 2, and explain why the quasielectron – described as an inverse quasihole – is singular. We recall in Section 3 the wavefunctions for the anyonic excitations on a lattice with N lattice points and their parent Hamiltonians. These wavefunctions are not singular for finite N . In Section 4.1, we approach the continuum limit by increasing the number of the lattice points N , while keeping the number of electrons and the number of magnetic fluxes in the system constant. We consider different positions of the quasielectron in relation to the lattice sites. In particular, we explain that, when we put the quasielectron on top of a lattice site, it leads to a finite trial wavefunction. In Section 4.2, we identify the terms that diverge in the continuum limit. We show that the ratio of the contributions from the divergent and regular terms is proportional to $\ln N$. This means that the continuum quasielectron is singular and is not confined to the LLL. The slow nature of this divergence makes it hard for detection in the numerics. We numerically show that indeed only the divergent terms are responsible for bringing about the most amount of change in the physical observables (e.g., excess charge) as we approach the continuum limit.

To remove the singularity we project the quasielectron on the LLL. We study this modified divergence free ansatz in Section 5, and explain how this also does not possess the topological properties expected for an anyonic quasielectron. In Section 5.1.1 we show that the anyon statistics obtained by moving a LLL-projected quasielectron adiabatically around a quasihole is different from the one obtained by moving the quasihole around the same quasielectron. The Berry phase obtained by moving the LLL-projected quasielectron around a quasihole depends on the size and shape of the contour. Moreover, in Section 5.1.2, we demonstrate that, if starting from the ansatz wavefunction with a quasihole and a LLL-projected quasielectron we take the position of the quasielectron to infinity, we fail to retrieve the wavefunction for an isolated quasihole.

2. Laughlin Wavefunction: Continuum Description

Consider a FQH droplet of filling fraction $1/q$ with M electrons, where q is a positive integer. To describe K quasiparticles at w_1, \dots, w_K , Laughlin introduced the following ansatz wavefunctions:

$$|\psi\rangle_{\text{cont}} = \mathcal{C}^{-1} \int \dots \int \prod_{i=1}^M d^2 Z_i |Z_1, \dots, Z_M\rangle \\ \times \prod_{i,k} (w_k - Z_i)^{pk} \prod_{i<j} (Z_i - Z_j)^q e^{-\sum_{i=1}^M |Z_i|^2 / 4l_B^2}, \quad (1)$$

where \mathcal{C} is a real normalization constant, the electronic coordinates Z_i take any value on the complex plane, and l_B is the magnetic length [6]. The Jastrow factor prevents

two particles from being at the same position. The state describes fermions for q odd and hardcore bosons for q even.

There are two types of quasiparticles in the FQHE, namely the quasihole and the quasielectron with fractional charges $+e/q$ and $-e/q$, respectively. Here $e > 0$ is the absolute value of the electronic charge. In Equation (1), $p_k = 0$ for all k , produces the Laughlin FQHE ground state wavefunction. When $p_k = +1$, there is a quasihole at w_k , where the additional (local in w_k) factor $\prod_i (w_k - Z_i)$ corresponds to the insertion of a positive flux tube at w_k [6].

However, the wavefunction is not physical when $p_k = -1$. The factor corresponding to the insertion of a negative flux tube at w_k is singular, when any of the electronic coordinates Z_i are equal to w_k . This renders the naive description of the quasielectron to be an inverse quasihole invalid.

3. Lattice Wavefunctions and Hamiltonians

In this section, we recall the salient features of the quasielectron wavefunction on a lattice, which was introduced in Ref. [18]. The lattice sites are z_i for $i = 1, \dots, N$. Here we consider the case of a square lattice with a roughly circular boundary of radius R . The local basis on site i is labelled by $|n_i\rangle$, where the lattice occupancy n_i is either 0 or 1. After setting the magnetic length $l_B = 1$, it is possible to write down the wavefunction for K different quasiparticles at the positions w_1, \dots, w_K in terms of the chiral correlator of CFT vertex operators as follows:

$$|\psi\rangle \propto \sum_{n_1, \dots, n_N} \langle 0 | \prod_{k=1}^K W_{p_k} \prod_{i=1}^N V_{n_i} | 0 \rangle |n_1, \dots, n_N\rangle, \quad (2)$$

where the vertex operators are

$$\begin{aligned} W_{p_k} &= : e^{ip_k \phi(w_j)/\sqrt{q}} :, \\ V_{n_j} &= \chi_{n_j} : e^{i(qn_j - \eta)\phi(z_j)/\sqrt{q}} :. \end{aligned} \quad (3)$$

Here $: \dots :$ denotes normal ordering, $\phi(z_j)$ is the chiral field of a massless free boson evaluated at the position z_j , χ_{n_j} are the unspecified single particle phase factors that do not depend on the w_j , and the area assigned per single lattice site is $2\pi\eta$. The vertex operator W_{p_k} with $p_k = +1$ (-1) creates a quasihole (quasielectron).

From Equation (2), we obtain the following ansatz for the K quasiparticle excitations at the positions w_1, \dots, w_K :

$$|\psi\rangle = \mathcal{C}^{-1} \sum_{n_1, \dots, n_N} \delta_n \prod_{i=1}^N \chi_{n_i} \prod_{i,k} (w_k - z_i)^{p_k n_i} \prod_{i < j} (z_i - z_j)^{q n_i n_j - \eta(n_i + n_j)} |n_1, \dots, n_N\rangle, \quad (4)$$

where the unspecified single particle phase factors are written as

$$\chi_{n_i} = e^{i(\phi_0 + \phi_j n_j)}, \quad \phi_0, \phi_j \in \mathbb{R}. \quad (5)$$

Note that the correlation function is zero unless the charge neutrality condition,

$$\sum_{i=1}^N n_i = \left(\eta N - \sum_{k=1}^K p_k \right) / q, \quad (6)$$

is obeyed by the lattice occupancies. This is imposed in Equation (4) by the Kronecker delta function δ_n . The real normalization constant \mathcal{C} in Equation (4) is a function of the quasiparticle positions, and it obeys

$$\mathcal{C}^2 = \sum_{n_1, \dots, n_N} \delta_n \prod_{k,j} |w_k - z_j|^{2p_k n_j} \prod_{i < j} |z_i - z_j|^{2q n_i n_j - 2\eta(n_i + n_j)} = \sum_{n_1, \dots, n_N} \delta_n \mathcal{C}_{n_1, \dots, n_N}^2. \quad (7)$$

Equation (4) provides a valid (finite) trial wavefunction. This ansatz also works when the quasielectron position w_k is arbitrarily close to a lattice site z_i . In this case, the proximity of w_k and z_i forces $n_i \rightarrow 1$. This allows us to include the infinitely large constant $(w_k - z_i)^{-1}$ in the normalization.

The charge neutrality condition described in Equation (6) guarantees that the number of particles in the FQH droplet remains constant for any η . This in turn means $N\eta = \text{constant}$, where N is the number of lattice sites inside the circle of fixed radius R . As we decrease η , R stays fixed, but the number of sites inside the circle increases, which allows the particles to be in more places. Thus the parameter η allows us to interpolate between the lattice limit ($\eta = 1$) and the continuum limit ($\eta \rightarrow 0^+$). In the continuum limit and with $p_k = 0$ for all k , starting from the wavefunction (4) defined on a lattice with uniformly distributed sites and a circular boundary, one obtains the Laughlin wavefunction. In the continuum limit, the occupied subset of lattice points (M of them) are the electronic coordinates Z_1, \dots, Z_M [22].

The wavefunction (4) is the exact ground state of the following few-body Hamiltonian [18]:

$$\begin{aligned} H &= \sum_{i=1}^N \hat{\Lambda}_i^\dagger \hat{\Lambda}_i, \\ \hat{\Lambda}_i &= \sum_{j(\neq i)} \frac{1}{z_i - z_j} \left[T_j^{-1} \hat{d}_j - T_i^{-1} \hat{d}_i (q \hat{n}_j - 1) \right], \\ T_k &= e^{i\phi_k} e^{-i\pi(k-1)} \prod_i (w_i - z_k)^{p_i} \prod_j (z_j - z_k)^{1-\eta}, \end{aligned} \quad (8)$$

where ϕ_k were introduced in Equation (5), \hat{d}_k is the hardcore fermionic (bosonic) annihilation operator acting on site k for q odd (even), and $\hat{n}_k = \hat{d}_k^\dagger \hat{d}_k$ is the number operator for the k th site. The above Equation (8) is a valid Hamiltonian as long as

$$\eta - \sum_i p_i / N < 1 + q / N. \quad (9)$$

This demonstrates that as we take the continuum limit there always exist few-body Hamiltonians, for which the wavefunctions (4) are exact ground states.

One can also compare the analytical states for $q = 2$ to the ground states of an interacting, bosonic Hofstadter model on a square lattice introduced in [23]. The model

allows nearest neighbor hopping, and the hopping terms are complex to mimic a uniform magnetic field. The on-site interactions are so strong that there is at most one boson on each site. For periodic boundary conditions, it was found in [24] that this model is in a topological phase for η less than about 0.4, and there is a high overlap with the lattice Laughlin states on a torus for η less than about 0.3. The analytical states can be obtained for periodic boundary conditions by evaluating the CFT correlator describing the state on the torus. This gives q states due to the topological degeneracy on the torus. In [18] it was found that the analytical states on a 6×6 square lattice on a torus with one quasihole, one quasielectron, $q = 2$, and three particles (giving $\eta = 1/6$) both have overlaps of 0.99 with the ground states of the interacting Hofstadter model with a positive and a negative pinning potential added to trap two anyons of opposite charge.

3.1. Braiding Statistics

When the k th anyon situated at w_k moves adiabatically in a closed contour c , the wavefunction is modified as $|\psi\rangle \rightarrow \mathbb{M}e^{i\theta_k}|\psi\rangle$. Here θ_k is the Berry phase, and the monodromy \mathbb{M} is the change in the wavefunction effected by only the analytical continuation.

For future use, we briefly repeat the computation of the Berry phase θ_k . Starting with the wavefunction (4) for K anyons, we write θ_k as follows:

$$\theta_k = i \oint_c \langle \psi | \frac{\partial \psi}{\partial w_k} \rangle dw_k + \text{c.c.} = \frac{i}{2} \oint_c \frac{1}{\mathcal{C}^2} \frac{\partial \mathcal{C}^2}{\partial w_k} dw_k + \text{c.c.} \quad (10)$$

From Equation (7) we observe that

$$\frac{\partial \mathcal{C}^2}{\partial w_k} = \sum_{n_1, \dots, n_N} \delta_n \mathcal{C}_{n_1, \dots, n_N}^2 \sum_j \frac{p_k n_j}{w_k - z_j}. \quad (11)$$

We also recall the following expression for the expectation value of an operator $\hat{\mathcal{O}}$ that is diagonal in the $|n_1, \dots, n_N\rangle$ basis:

$$\langle \psi | \hat{\mathcal{O}} | \psi \rangle = \frac{1}{\mathcal{C}^2} \sum_{n_1, \dots, n_N} \delta_n \mathcal{C}_{n_1, \dots, n_N}^2 \langle n_1, \dots, n_N | \hat{\mathcal{O}} | n_1, \dots, n_N \rangle. \quad (12)$$

Using Equations (10), (11), and (12), we obtain [25, 26]

$$\theta_k = i \frac{p_k}{2} \oint_c \sum_i \frac{\langle n_i \rangle}{w_k - z_i} dw_k + \text{c.c.} \quad (13)$$

When the quasiparticles are screened – i.e., a quasiparticle at w_j only affects the particle densities close to w_j (see Figure 2, for example) – it is possible to separate them sufficiently. We now move a quasiparticle at w_k in a closed contour c , such that w_j always remains far from c . One then writes the anyonic statistics γ of the k th and the j th quasiparticles as

$$\begin{aligned} 2\pi\gamma &= \theta_{k, (w_j \text{ inside})} - \theta_{k, (w_j \text{ outside})} \\ &= \frac{ip_k}{2} \oint_c \sum_i \frac{\langle n_i \rangle_{(w_j \text{ inside})} - \langle n_i \rangle_{(w_j \text{ outside})}}{w_k - z_i} dw_k + \text{c.c.}, \end{aligned} \quad (14)$$

where $\theta_{k,(w_j \text{ inside})}$ ($\theta_{k,(w_j \text{ outside})}$) is the Berry phase with the j th anyon inside (outside) c . In the above equation, we have used the fact that the monodromy \mathbb{M} is the identity.

For screened and well-separated anyons, $\langle n_i \rangle_{(w_j \text{ inside})} - \langle n_i \rangle_{(w_j \text{ outside})}$ is independent of w_k . It is non-zero only for lattice positions that are close to the two possible values of w_j . Using this in Equation (14), one obtains the anyon statistics

$$\gamma = p_j p_k / q, \quad (15)$$

which is the expected statistics for anyons in a model with the topology of the Laughlin state. We note that the above argument neither depends on the nature (whether they are quasiholes or quasielectrons) of the anyons, nor on the value of η .

4. Divergence of the Continuum Limit of the Lattice Wavefunction

For the sake of definiteness, we consider one quasielectron at w_1 and one quasihole at w_2 . We write the ansatz for this system using Equation (4) as follows:

$$|\psi\rangle = \mathcal{C}^{-1} \sum_{n_1, \dots, n_N} \delta_n \prod_{i=1}^N \chi_{n_i} \prod_{i=1}^N \left(\frac{w_2 - z_i}{w_1 - z_i} \right)^{n_i} \prod_{i < j} (z_i - z_j)^{q n_i n_j - \eta(n_i + n_j)} |n_1, \dots, n_N\rangle. \quad (16)$$

Note that, since $\sum_k p_k = 0$ in this system, we still have $M = N\eta/q$ particles.

4.1. Continuum Limit of the Quasielectron Ansatz: Numerics

In order to isolate and study the properties of the quasielectron, we consider w_1 to be the origin and w_2 to be the complex infinity. In the limit $w_2 \rightarrow \infty$, the factor $\prod_{i=1}^N (w_2 - z_i)^{n_i}$ approaches $\prod_{i=1}^N w_2^{n_i} = w_2^M$, which is a constant (albeit, an infinite one) that can be absorbed in the normalization. This gives the following wavefunction for a single quasielectron:

$$|\psi_{\text{QE}}\rangle = \mathcal{C}^{-1} \sum_{n_1, \dots, n_N} \delta_n \prod_{i=1}^N \tilde{\chi}_{n_i} \prod_{i=1}^N z_i^{-n_i} \prod_{i < j} (z_i - z_j)^{q n_i n_j - \eta(n_i + n_j)} |n_1, \dots, n_N\rangle, \quad (17)$$

where $\tilde{\chi}_{n_i} = (-1)^{n_i} \chi_{n_i}$.

We then proceed to study the continuum limit of the quasielectron ansatz (17) for a square lattice defined on a circular disk of radius $R \approx 5.6\sqrt{2\pi}$. Without loss of generality, we consider the following initial primitive lattice vectors:

$$\mathbf{a}_1 = \hat{x}\sqrt{2\pi}, \quad \mathbf{a}_2 = \hat{y}\sqrt{2\pi}, \quad (18)$$

where \hat{x} and \hat{y} are the unit vectors in the x and y directions. Since the area per primitive cell needs to be $2\pi\eta$, we initially have $\eta = 1$. The circular disk initially contains 96 lattice points.

We gradually decrease η while keeping M and $N\eta$ fixed. To achieve this, in the next step we consider a square lattice in which we replace each of the unit cells in the original lattice with L^2 smaller unit cells each having the area $2\pi/L^2$. In this way one has

$$N = N_{\text{New}}/L^2, \quad \eta = L^2\eta_{\text{New}}, \quad N_{\text{New}}\eta_{\text{New}} = N\eta. \quad (19)$$

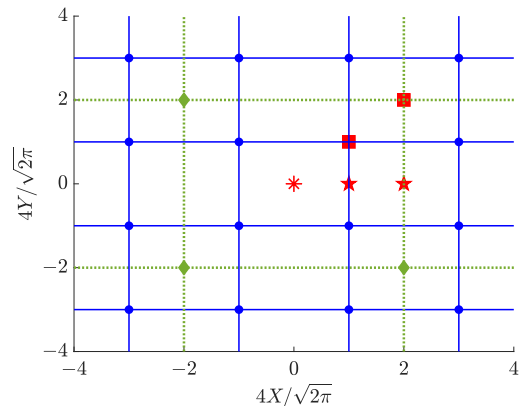


Figure 1. A step toward the continuum limit for a square lattice. We start with a square lattice (green diamonds), where the length of the primitive lattice vector is $\sqrt{2\pi}$. In the next step (new lattice points are the blue dots), the length of the primitive lattice vector becomes $\sqrt{\pi/2}$, and we have four times as many lattice sites inside the same area. The three inequivalent quasielectron positions that we consider (cf. Figure 5) are – (1) the center of a square plaquette formed by four lattice points (red asterisk), (2) midway between two lattice sites (red pentagon), and (3) on a lattice point (red square).

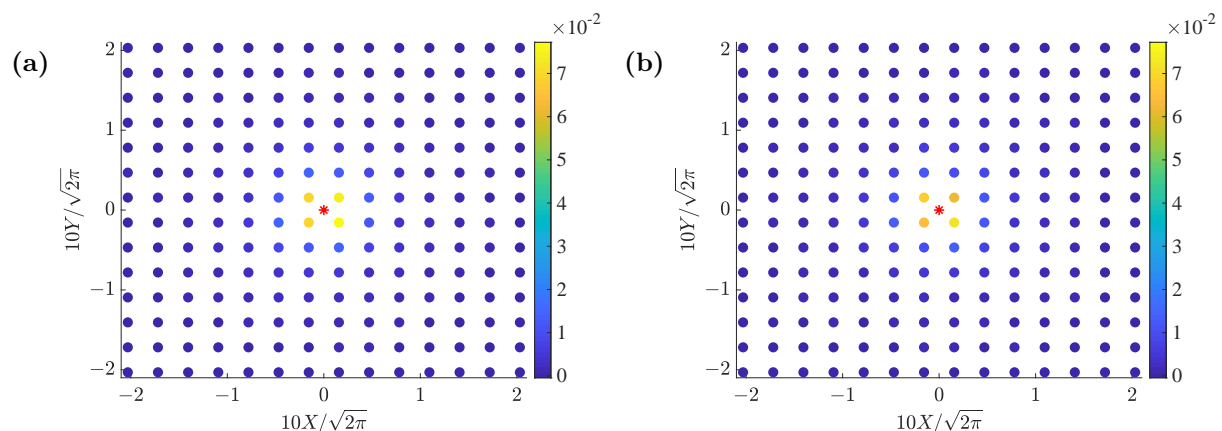


Figure 2. Excess particle densities $\langle n_i \rangle_{-1} - \langle n_i \rangle_0$ (see below Equation (21) for the definitions of $\langle n_i \rangle_{-1}$ and $\langle n_i \rangle_0$) at different lattice points in the presence of a quasielectron (17), shown by the red star at the origin, for inverse filling fractions $q = 2$ (a), and $q = 3$ (b). Here we only show a part of the lattice. The particle densities of only a few lattice sites close to the quasielectron are affected. The screened nature of the quasielectron shows that the quasiparticles described by Equation (4) have the braiding properties Equation (15), see Section 3.1.

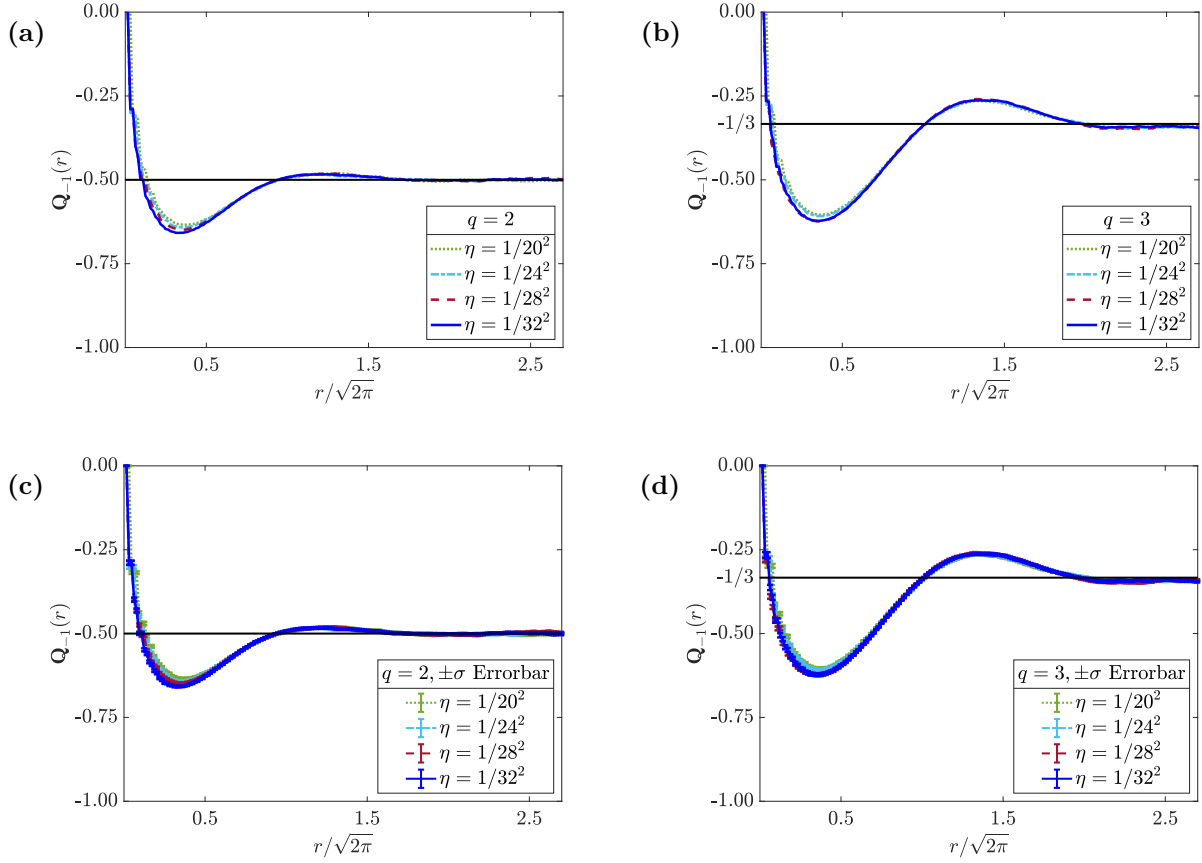


Figure 3. Excess charge $\mathbf{Q}_{-1}(r)$ of the quasielectron (17) for inverse filling fractions $q = 2$ [(a) and (c)] and $q = 3$ [(b) and (d)]. The quasielectron is at the origin of a circular disk of radius $R \approx 5.6\sqrt{2\pi}$ with a square lattice with N lattice points embedded on it. We define $\mathbf{Q}_{-1}(r)$ as a function of the radial distance r from the quasielectron in the units of absolute electronic charge e in Equation (20). We show the $\mathbf{Q}_{-1}(r)$ averaged over 25 different Monte Carlo datasets in (a) and (b). Additionally, in (c) and (d), we include an errorbar of $\pm\sigma$ for the excess charge profiles, where σ is the variance of $\mathbf{Q}_{-1}(r)$. To approach the continuum, starting from the lattice limit $\eta = 1$, in consecutive steps we decrease η as $\eta = 1/L^2$, and put L^2N lattice sites on the same circular disk of radius R . We show the $\mathbf{Q}_{-1}(r)$ profiles for $L = 20, 24, 28$, and 32 . For $r \gtrsim 2\sqrt{2\pi}$, for all the η values shown here, the excess charge for the quasielectron at filling fractions $1/q$ is indeed close to $1/q$. When r is small, i.e., near the trough of the excess charge profile, $\mathbf{Q}_{-1}(r)$ goes down as we decrease η . It is hard to conclude if the profile has reached a limit or not after including the $\pm\sigma$ errorbar. In Section 4.2, we argue that the curves do not converge.

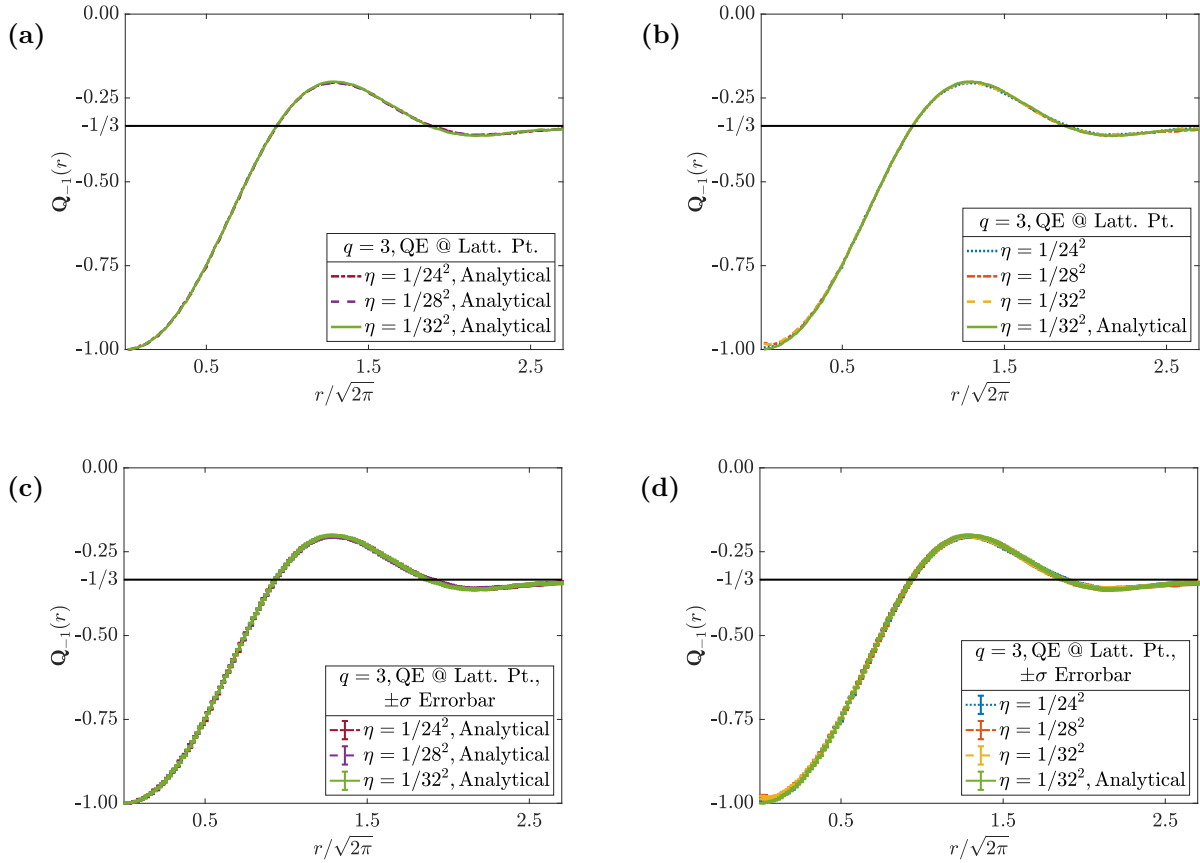


Figure 4. Excess charge $Q_{-1}(r)$ profile with the quasielectron on a lattice site for $q = 3$. In (a), we plot $Q_{-1}(r)$ for $\eta = 1/24^2, 1/28^2$, and $1/32^2$ using the exact analytical wavefunction, where we always keep the lattice site at $\sqrt{2\pi\eta}(1/2, 1/2)$ occupied. The convergence of $Q_{-1}(r)$ is clearly demonstrated here. In (b), we compare the excess charge profile for $\eta = 1/32^2$ obtained from the analytical wavefunction to the ones, with $\eta = 1/24^2, 1/28^2$, and $1/32^2$, obtained from the wavefunction with the quasielectron close to a lattice site at $w = \sqrt{2\pi}(\sqrt{\eta}/2, \sqrt{\eta}/2 - 10^{-4})$. In (c) and (d), we show (a) and (b) with $\pm\sigma$ errorbars, respectively.

As shown in Figure 1, we shall consider three distinct positions of the quasielectron – (1) the center of a square plaquette formed by four lattice sites, (2) midway between two lattice sites, and (3) on a lattice point. We place the origin at (1). As we decrease η and increase N while keeping $N\eta$ constant, (2) and (3) converge to the origin. In the continuum limit, all the three inequivalent quasielectron positions coincide.

We already explained below Equation (7) that putting the quasielectron on top of a lattice site [position (3)] obtains a finite trial wavefunction. That explanation also holds in the continuum limit. However, such reasoning does not work, when the quasielectron is at the center of a square plaquette [position (1)], or midway between two lattice sites [position (2)]. The question is if the continuum trial wavefunctions, with the quasielectron in the above three inequivalent positions, coincide and converge. At the continuum limit, one defines the LLL. Laughlin states and their quasiparticle

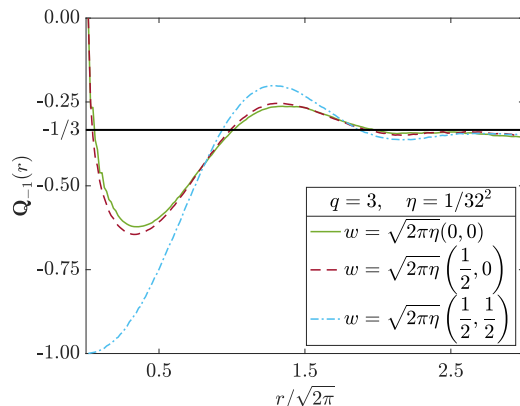


Figure 5. Excess charge profiles for $q = 3$ and $\eta = 1/32^2$ with three different inequivalent positions w of the quasielectron in the square lattice. Here r is the radial distance from the quasielectron position. The three positions – center of a square plaquette (solid green), midpoint of a side (brown dashed), and on top of a lattice site (indigo dash-dot) – lead to different $\mathbf{Q}_{-1}(r)$ profiles.

excitations should be confined to it. We need to verify this as well.

We study the excess charge profile, which is defined as follows:

$$\mathbf{Q}_{-1}(r) = \sum_{i=1}^N \Theta(r - |z_i|) (\langle n_i \rangle_0 - \langle n_i \rangle_{-1}). \quad (20)$$

Here $\Theta(x)$ denotes the Heaviside step function

$$\Theta(x) = \begin{cases} 0 & \text{for } x < 0 \\ 1 & \text{otherwise} \end{cases}. \quad (21)$$

In Equation (20), $\langle n_i \rangle_{-1}$ are the occupancies of the lattice sites with the quasielectron ansatz (17), and $\langle n_i \rangle_0$ are the occupancies of the lattice sites calculated with the wavefunction (4) and all $p_k = 0$. In Figures 2a and 2b, we show the excess particle densities ($\langle n_i \rangle_{-1} - \langle n_i \rangle_0$) for $q = 2$ and $q = 3$.

We have considered a quasielectron at the center of a square plaquette down to $\eta = 1/32^2$ for both $q = 2$ and 3 in Figure 3. Here we go to much smaller values of η than what was considered in Ref. [18]. The smallest value considered there was $\eta = 1/10^2$. The excess charge, as expected, saturates to $\mathbf{Q}_{-1}(r) = -1/q$ in both Figures 3a and 3b for $r \gtrsim 2.0\sqrt{2\pi}$. For distances smaller than $\sqrt{2\pi}$, especially near the trough of the excess charge profile, it keeps going down as we decrease η . However, the amount of change is so small – keeping in mind the numerical accuracy of our calculations (see Figures 3c and 3d, where we have included the $\pm\sigma$ errorbar) – that it is difficult to comment whether the charge profile has saturated or not.

On the other hand in Figures 4a and 4c (in the latter we have included $\pm\sigma$ errorbars), we show the converged (unlike Figure 3) excess charge profiles for small values of η using the exact ansatz wavefunction for the quasielectron position $w =$

$\sqrt{2\pi\eta}(1/2, 1/2)$. We keep the above lattice site always occupied to obtain $\mathbf{Q}_{-1}(r)$ with the exact ansatz while performing the Monte Carlo simulations. In Figures 4b and 4d (the latter shows $\pm\sigma$ errorbars), we compare $\mathbf{Q}_{-1}(r)$ calculated with the exact analytical ansatz to the one obtained by keeping the quasielectron close to a lattice point $\sqrt{2\pi\eta}(1/2, 1/2)$. In Figure 5, we plot the $\mathbf{Q}_{-1}(r)$ for the three different quasielectron positions shown in Figure 1.

Figures 2, 3, 4, and 5 demonstrate that the quasielectron is indeed screened. Combining this with the arguments of Section 3.1 shows that the quasielectron described by Equation (4) also has the braiding properties expected for anyonic quasielectrons.

4.2. Divergence of the Continuum Quasielectron: Analytical Argument

The foregoing numerical calculation could not definitively answer if the quasielectron (17) leads to a singularity in the continuum, when it is placed at the center of a square plaquette or midway between two lattice points. We therefore take recourse to an analytical argument. When we are close to the continuum limit, there are so many lattice points that the electrons can be almost anywhere. However, at the place where we have the singularity, the difference between the lattice and the continuum is important.

In particular, the underlying lattice structure introduces a distance of closest approach from the quasielectron position ξ (as long as the quasielectron is not placed on top of a lattice point). Since the length of the primitive lattice vectors in the square lattice is $\sqrt{2\pi\eta}$, we have

$$\xi \propto \sqrt{\eta} \propto 1/\sqrt{N}. \quad (22)$$

The proportionality constant in Equation (22) depends on the position of the quasielectron with respect to a square plaquette.

In the continuum, the LLL is well-defined and the quasielectron should be entirely confined to it. This does not hold for the wavefunction (17) because of the $1/z_i$ factors. We write the norm of the single electron LLL wavefunction $e^{-|Z|^2/4}$ multiplied by the quasielectron pole $1/Z$ over a domain with a hole around the singularity as follows:

$$\int \int_{D'} \left| \frac{e^{-|Z|^2/4}}{Z} \right|^2 d^2Z = \int \int_D \Theta^2(|Z| - \xi) \left| \frac{e^{-|Z|^2/4}}{Z} \right|^2 d^2Z, \quad (23)$$

where $\Theta(x)$ is the Heaviside step function (21). We perform the integral in the left hand side on a sufficiently large disk D with a small hole of radius ξ around the position of the quasielectron – the origin. We denote this not-simply-connected domain as D' . The integral on the right hand side, with the wavefunction $\Theta(|Z| - \xi) e^{-|Z|^2/4}/Z$, is performed on the full disk. The wavefunctions in both sides of Equation (23) do not live in the LLL.

The preceding discussion establishes that the lattice quasielectron (17) tends to the following continuum quasielectron living on D' :

$$|\psi_{\text{QE}}\rangle_{\text{cont}} = \mathcal{C}^{-1} \int \cdots \int_{D'^M} \prod_{i=1}^M d^2Z_i |Z_1, \dots, Z_M\rangle \prod_i Z_i^{-1} \prod_{i<j} (Z_i - Z_j)^q e^{-\sum_{i=1}^M |Z_i|^2/4t_B^2}. \quad (24)$$

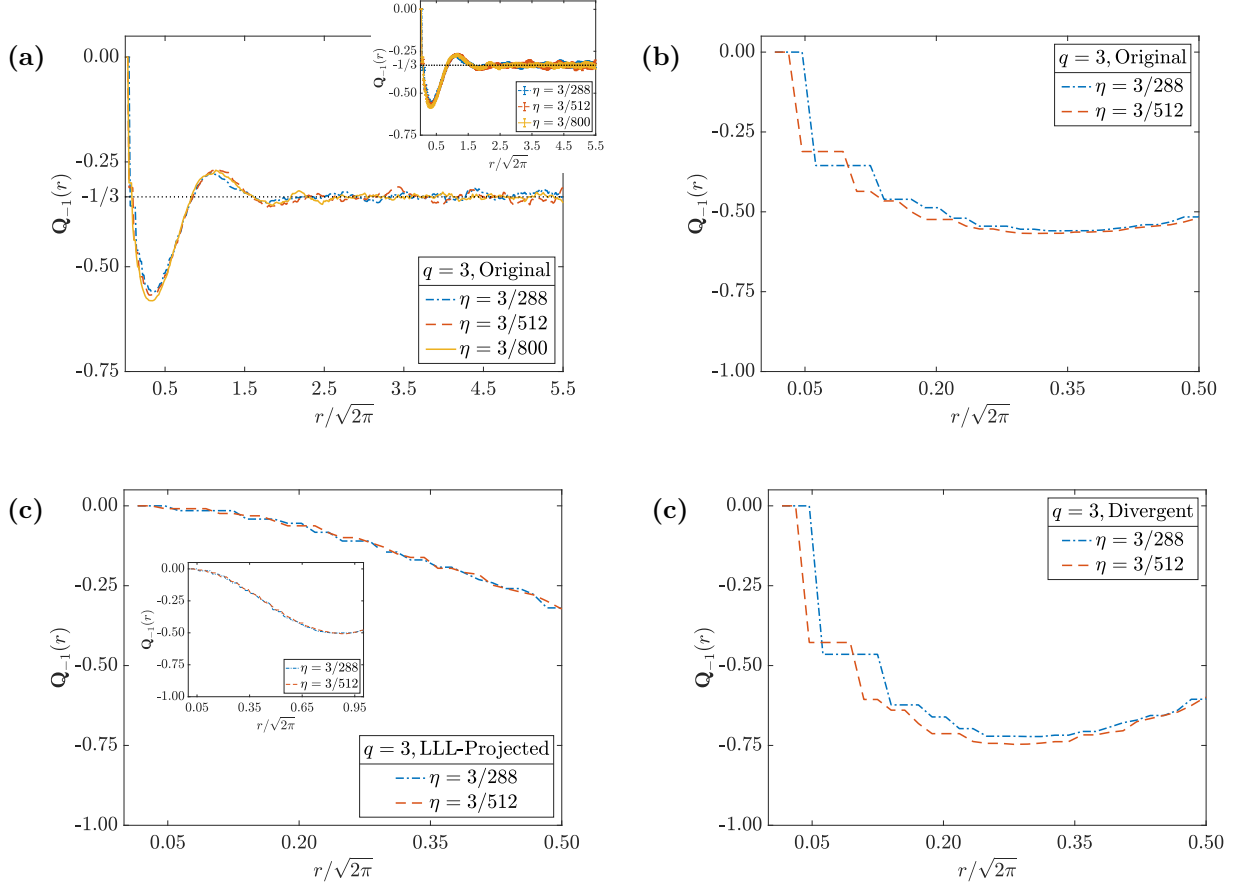


Figure 6. The divergent terms in the expansion of Equation (17) [the terms that are not confined to the LLL in the continuum – i.e., the ones left after subtracting Equation (44) from (17)] are responsible for the changes in $\mathbf{Q}_{-1}(r)$ between $0 < r \lesssim \sqrt{2\pi}$. All of these plots are for a square lattice on a circular disk of radius $R \approx 8.3\sqrt{2\pi}$ and $q = 3$. We plot $\mathbf{Q}_{-1}(r)$ vs. r with ansatz (17) for $\eta = 3/288, 3/512$, and $3/800$ in (a). As we decrease η , the minimum of $\mathbf{Q}_{-1}(r)$ near $r = 0.25\sqrt{2\pi}$ keeps decreasing. The oscillations about $\mathbf{Q}_{-1}(r) = -1/3$ for $r \gtrsim 2.0\sqrt{2\pi}$ gradually decrease with decreasing η . We have included the $\pm\sigma$ errorbars in the inset of (a). In (b), (c), and (d) we show the $\mathbf{Q}_{-1}(r)$ vs. r plots for $\eta = 3/288$ and $3/512$, where we compute the excess charges with the ansatz (17), with ansatz (17) projected to the LLL [i.e., with ansatz (44)], and with only the divergent terms in Equation (17), respectively. From (c), we notice that $\mathbf{Q}_{-1}(r)$ calculated with Equation (44) for the two different values of η are almost identical. The inset of (c) shows $\mathbf{Q}_{-1}(r)$ for upto $r = \sqrt{2\pi}$. In both (b) and (d), there are significant changes in $\mathbf{Q}_{-1}(r)$ when η changes.

Expanding the product $\prod_{i<j} (Z_i - Z_j)^q$, we write the wavefunction (24) as follows:

$$|\psi_{\text{QE}}\rangle_{\text{cont}} = \mathcal{C}^{-1} \int \cdots \int_{D'^M} \prod_{i=1}^M d^2 Z_i |Z_1, \dots, Z_M\rangle \sum_{q_1, \dots, q_M} \mathcal{E}_{q_1, \dots, q_M} \prod_{l=1}^M Z_l^{q_l - 1} e^{-\frac{|Z_l|^2}{4}}, \quad (25)$$

where $\mathcal{E}_{q_1, \dots, q_M}$ are different expansion coefficients, and q_1, \dots, q_M satisfy

$$\sum_l q_l = qM(M-1)/2, \quad 0 \leq q_l \leq (M-1)q. \quad (26)$$

Note that $\mathcal{E}_{q_1, \dots, q_M}$ are the same coefficients that appear in the expansion of the Laughlin wavefunction (Equation (1) with all $p_k = 0$) in the basis $|q_1, \dots, q_M\rangle$ of single electron wavefunction product, which we write as follows:

$$|\psi\rangle = \mathcal{C}^{-1} \sum_{q_1, \dots, q_M} \mathcal{E}_{q_1, \dots, q_M} |q_1, \dots, q_M\rangle. \quad (27)$$

To go back to the coordinate basis $|Z_1, \dots, Z_M\rangle$, one needs to insert the following identity operator,

$$\mathbb{1} = \int \cdots \int_{D^M} \prod_{i=1}^M d^2 Z_i |Z_1, \dots, Z_M\rangle \langle Z_1, \dots, Z_M|, \quad (28)$$

in Equation (27), and use

$$\langle Z_1, \dots, Z_M | q_1, \dots, q_M \rangle \propto \prod_{l=1}^M Z_l^{q_l} e^{-\frac{|Z_l|^2}{4}}. \quad (29)$$

Using this, we write Equation (25) as:

$$|\psi_{\text{QE}}\rangle_{\text{cont}} = \mathcal{C}^{-1} \sum_{q_1, \dots, q_M} \mathcal{E}_{q_1, \dots, q_M} |q_1 - 1, \dots, q_M - 1\rangle, \quad (30)$$

where $|q_1 - 1, \dots, q_M - 1\rangle$ is an orthonormal product basis similar to $|q_1, \dots, q_M\rangle$. This new single electron basis on D' , however, includes the element $|-1\rangle$ with

$$\langle Z | -1 \rangle \propto Z^{-1} e^{-\frac{|Z|^2}{4}}, \quad (31)$$

to accommodate the quasielectron pole. Note that the function (31) is normalizable on the domain D' .

We have two types of terms in the expansion (25) – the ones with all the q_l positive, and the ones with at least one of them equal to zero. The first type of terms $\{q_1^{\text{reg}}, \dots, q_M^{\text{reg}}\}$ do not lead to any singularity. We delineate this regular (not normalized) part of the continuum quasielectron wavefunction (25) as follows:

$$|\psi_{\text{QE}}^{\text{reg}}\rangle_{\text{cont}} = \mathcal{C}^{-1} \int \cdots \int_{D'^M} \prod_{i=1}^M d^2 Z_i |Z_1, \dots, Z_M\rangle \sum_{q_1^{\text{reg}}, \dots, q_M^{\text{reg}}} \mathcal{E}_{q_1^{\text{reg}}, \dots, q_M^{\text{reg}}} \prod_{l=1}^M Z_l^{q_l^{\text{reg}} - 1} e^{-\frac{|Z_l|^2}{4}}, \quad (32)$$

where \mathcal{C} is the same as in Equations (24) and (25).

The second type of terms $\{q_1^\infty, \dots, q_M^\infty\}$ however, have at least one pole at the origin. Among all these terms, those that have poles of the type Z_k^{-1} , must have $q_k = 0$ in Equation (25). Factors of Z_k appear in $\prod_{i<j} (Z_i - Z_j)^q$ either from $\prod_{l(<k)} (Z_l - Z_k)^q$,

or from $\prod_{l(>k)} (Z_k - Z_l)^q$. Note that both the binomial expansions of $(Z_l - Z_k)^q$ and $(Z_k - Z_l)^q$ produce homogeneous polynomials of degree q . The only monomial in these expansions with no powers of Z_k is Z_l^q . This also shows that it is not possible to have two q_l to be equal to zero.

Using this we write the singular (not normalized) part of the continuum quasielectron wavefunction (24) as follows:

$$\begin{aligned} |\psi_{\text{QE}}^\infty\rangle_{\text{cont}} &= \mathcal{C}^{-1} \int \cdots \int_{D'^M} \prod_{i=1}^M d^2 Z_i |Z_1, \dots, Z_M\rangle \\ &\times \sum_{k=1}^M Z_k^{-1} \prod_{l(<k)} Z_l^{q-1} \prod_{l(>k)} (-Z_l)^{q-1} \prod_{\substack{i<j \\ i,j \neq k}} (Z_i - Z_j)^q e^{-\frac{|Z_j|^2}{4}}, \end{aligned} \quad (33)$$

where \mathcal{C} is the same as in Equations (24), (25), and (32). After cancellation only one of these poles in $\prod_l Z_l^{-1}$ remain in the singular terms (33). The other poles coming from $\prod_{l(\neq k)} Z_l^{-1}$, in the term that has a residual pole Z_k^{-1} , reduce the power of Z_l from q to $q-1$. Denoting the $\{q_1^\infty, \dots, q_M^\infty\}$ with $q_k = 0$ as $\{q_1^{k\infty}, \dots, q_M^{k\infty}\}$ we finally write Equation (33) as follows:

$$\begin{aligned} |\psi_{\text{QE}}^\infty\rangle_{\text{cont}} &= \mathcal{C}^{-1} \int \cdots \int_{D'^M} \prod_{i=1}^M d^2 Z_i |Z_1, \dots, Z_M\rangle \sum_{k=1}^M Z_k^{-1} \\ &\times \sum_{q_1^{k\infty}, \dots, q_M^{k\infty}} \mathcal{E}_{q_1^{k\infty}, \dots, q_M^{k\infty}} \prod_{l(\neq k)} Z_l^{q_l^{k\infty}-1} e^{-\frac{|Z_l|^2}{4}}. \end{aligned} \quad (34)$$

Using the orthogonality of the basis elements in the right hand side of Equation (30), and Equations (32) and (34), we derive the following normalization condition for the wavefunction (25):

$$\mathcal{C}_{\text{reg}}^2 + \mathcal{C}_\infty^2 = \mathcal{C}^2, \quad (35)$$

where

$$\mathcal{C}_{\text{reg}}^2 = \sum_{q_1^{\text{reg}}, \dots, q_M^{\text{reg}}} \mathcal{E}_{q_1^{\text{reg}}, \dots, q_M^{\text{reg}}}^2 \prod_{l=1}^M \int \int_{D'} d^2 Z_l |Z_l|^{2(q_l^{\text{reg}}-1)} e^{-\frac{|Z_l|^2}{2}}, \quad (36)$$

and

$$\begin{aligned} \mathcal{C}_\infty^2 &= \sum_{k=1}^M \int \int_{D'} d^2 Z_k \frac{1}{|Z_k|^2} e^{-\frac{|Z_k|^2}{2}} \\ &\times \sum_{q_1^{k\infty}, \dots, q_M^{k\infty}} \mathcal{E}_{q_1^{k\infty}, \dots, q_M^{k\infty}}^2 \prod_{l(\neq k)} \int \int_{D'} d^2 Z_l |Z_l|^{2(q_l^{k\infty}-1)} e^{-\frac{|Z_l|^2}{2}}. \end{aligned} \quad (37)$$

The integrands of the type $|Z_l|^{2(q_l-1)} e^{-\frac{|Z_l|^2}{2}}$ lead to the following radial integrals:

$$\int_0^\infty r_l^{2q_l-1} e^{-r_l^2/2} dr = 2^{q_l-1} \Gamma(q_l), \quad (38)$$

where in the $\xi \rightarrow 0$ limit we have simply replaced ξ by zero. The integrands of the type $|Z_k|^{-2}e^{-\frac{|Z_k|^2}{2}}$ in Equation (37), on the other hand, lead to

$$\int_{\xi}^{\infty} \frac{1}{r} e^{-r^2/2} dr = \frac{1}{2} E_1 \left(\frac{\xi^2}{2} \right), \quad (39)$$

where $\xi \propto 1/\sqrt{N}$ is the distance of closest approach between the electrons and the singularity, and $E_1(x)$ is the exponential integral [27]. To estimate the exponential integral we use the following bound:

$$\frac{1}{2} e^{-x} \ln \left(1 + \frac{2}{x} \right) < E_1(x) < e^{-x} \ln \left(1 + \frac{1}{x} \right), \quad (40)$$

where $x > 0$.

For comparing the contribution of the regular terms with the contribution of the irregular terms with poles, we introduce the following (always positive) ratio:

$$r = \frac{\mathcal{C}_{\infty}^2}{\mathcal{C}_{\text{reg}}^2} = \frac{1}{2} E_1 \left(\frac{\xi^2}{2} \right) r_*(M), \quad (41)$$

where $r_*(M)$ denotes a function of M . In the above, we have used that each term of the sum \sum_k in the right hand side of Equation (37) is proportional to $E_1(\xi^2/2)/2$. From Equations (40) and (41), we show that in the continuum limit the contribution from the pole (37) diverges as $\ln N$, when the quasielectron is situated either at the center of a square plaquette or midway between two lattice sites. The slow nature of the singularity is indeed difficult to capture in numerics.

Consistent with the above analysis, we numerically demonstrate that in the divergence of the excess charge $\mathbf{Q}_{-1}(r)$ the irregular terms (the ones leading to a pole in the continuum and hence not confined to the LLL) in ansatz (17) play the most important part. Here we are concerned about the continuous lowering of the $\mathbf{Q}_{-1}(r)$ profile near the minima close to $r = 0.25\sqrt{2\pi}$. The other parts of the profile eventually converge. In particular, the oscillations for $r \gtrsim 2.0\sqrt{2\pi}$ due to the underlying lattice structure die off, see Figure 6a. With the help of Figures 6b, 6c, and 6d we show that, when we decrease η , the $\mathbf{Q}_{-1}(r)$ profile between $0 < r \lesssim \sqrt{2\pi}$ is most affected by the aforementioned divergent terms.

5. Properties of the LLL-Projected Quasielectron Ansatz

The obvious way to remove the singularity at the quasielectron position w_1 from the ansatz (17) is to project it to the LLL. We do this by removing the singular terms, which amounts to subtracting the following terms from $\prod_{i < j} (z_i - z_j)^{q^{n_i n_j}}$:

$$\mathcal{R} = \sum_{k=1}^N n_k \prod_{l(>k)} (w_1 - z_l)^{q^{n_l n_k}} \prod_{l(<k)} (z_l - w_1)^{q^{n_k n_l}} \prod_{\substack{i < j \\ i, j \neq k}} (z_i - z_j)^{q^{n_i n_j}}. \quad (42)$$

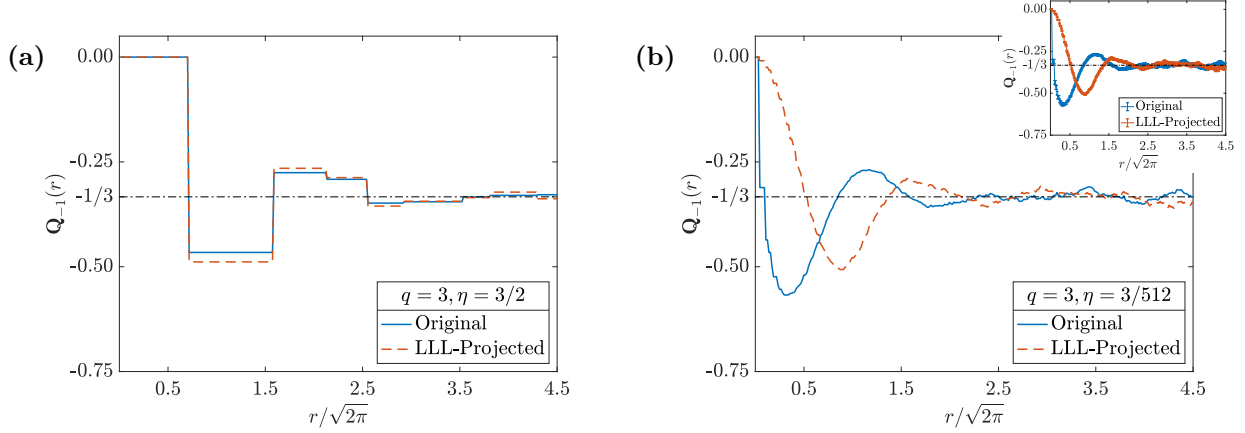


Figure 7. Comparison of the excess charge $\mathbf{Q}_{-1}(r)$ for the quasielectron, calculated with the original quasielectron ansatz (17) [blue solid] and the modified divergence-free ansatz (44) [red dashed]. Both of them are for a square lattice on a circular disk of radius $R \approx 8.3\sqrt{2\pi}$ and inverse filling fraction $q = 3$. We have $\eta = q/2$ in (a), and $\eta = q/(2 \times 16^2)$ in (b) [$\pm\sigma$ errorbar in the inset]. Already in (a) the excess charge profiles do not match fully. For large r , however, we observe that $\mathbf{Q}_{-1}(r) \rightarrow 1/q$ for all the profiles.

Comparing Equation (42) with Equation (33), we note that it is equivalent to subtracting the following from $\prod_{i<j} (Z_i - Z_j)^q$ in the continuum limit:

$$\mathcal{R}_{\text{cont}} = \sum_{k=1}^M \prod_{l(>k)} (w_1 - Z_l)^q \prod_{l(<k)} (Z_l - w_1)^q \prod_{\substack{i<j \\ i,j \neq k}} (Z_i - Z_j)^q. \quad (43)$$

Using this we write the modified lattice ansatz for a single quasielectron as follows:

$$|\psi_{\text{QE}}\rangle = \mathcal{C}^{-1} \sum_{n_1, \dots, n_N} \delta_n \prod_{i=1}^N \chi_{n_i} \prod_{i=1}^N (w_1 - z_i)^{-n_i} (1 - \mathcal{F}) \times \prod_{i<j} (z_i - z_j)^{qn_i n_j - \eta(n_i + n_j)} |n_1, \dots, n_N\rangle, \quad (44)$$

where we use phase factors χ_{n_i} similar to Equation (16), and use the following definition for \mathcal{F} :

$$\mathcal{F} = \mathcal{R} \prod_{i<j} (z_i - z_j)^{-qn_i n_j} = \sum_k n_k \prod_{l(\neq k)} \left(\frac{w_1 - z_l}{z_k - z_l} \right)^{qn_l n_k}. \quad (45)$$

Incorporating the above modification, one writes the ansatz for a quasielectron at w_1 and a quasihole at w_2 as follows:

$$|\psi\rangle = \mathcal{C}^{-1} \sum_{n_1, \dots, n_N} \delta_n \prod_{i=1}^N \chi_{n_i} \prod_{i=1}^N (w_1 - z_i)^{-n_i} (1 - \mathcal{F}) \prod_{i=1}^N (w_2 - z_i)^{n_i} \times \prod_{i<j} (z_i - z_j)^{qn_i n_j - \eta(n_i + n_j)} |n_1, \dots, n_N\rangle, \quad (46)$$

where we have kept the multiplicative factor for the quasihole $\prod_{i=1}^N (w_2 - z_i)^{n_i}$ unchanged.

We numerically study the excess charge profiles with the modified divergence-free quasielectron (44) in Figure 7. It is known that for $\eta = q/2$ the quasielectron excess charge is precisely the negative of the quasihole excess charge [18]. For this special value of η we see that the original quasielectron (17) and the modified divergence-free quasielectron (44) produce almost similar profiles for $\mathbf{Q}_{-1}(r)$. However, as we move away from this special η value and move toward the continuum limit, the difference between the two quasielectrons becomes more apparent. However, for large r we observe $\mathbf{Q}_{-1}(r) \rightarrow 1/q$ for both quasielectrons. We now demonstrate that the LLL-projected quasielectron does not have the properties expected for anyons hosted in systems with the topology of the Laughlin state.

5.1. Inconsistencies in the Modified Ansatz

In this section we first show that the modified ansatz does not give rise to the braiding properties Equation (15). We further demonstrate that starting from the ansatz for an FQH system with a quasihole and a modified quasielectron it is not possible to isolate a quasihole.

5.1.1. Braiding Statistics To determine the braiding statistics between a quasihole and the modified quasielectron, we need to obtain the Berry phases from the wavefunction (46). We write the normalization constant there as follows:

$$\mathcal{C}^2 = \sum_{n_1, \dots, n_N} \delta_n \prod_i |w_1 - z_i|^{-2n_i} |w_2 - z_i|^{2n_j} \prod_{i < j} |z_i - z_j|^{2qn_i n_j - 2\eta(n_i + n_j)} |1 - \mathcal{F}|^2. \quad (47)$$

Following the same steps delineated in Section 3.1, we obtain the Berry phase by moving the quasihole coordinate w_2 in a loop as follows:

$$\theta_2 = \frac{i}{2} \oint_c \sum_i \frac{\langle n_i \rangle}{w_2 - z_i} dw_2 + \text{c.c.}, \quad (48)$$

where we have used the fact that \mathcal{F} is w_2 independent. Using this expression for the Berry phase, and the fact that both the quasihole and modified quasielectron are localized, we obtain the anyonic statistics between the quasihole and the quasielectron to be $\gamma = -1/q$.

We then proceed to calculate the Berry phase by moving the quasielectron coordinate w_1 in a loop and obtain

$$\theta_1 = -\frac{i}{2} \oint_c \sum_i \frac{\langle n_i \rangle}{w_1 - z_i} dw_1 - \frac{i}{2} \oint_c \left\langle \frac{1}{1 - \mathcal{F}} \frac{\partial \mathcal{F}}{\partial w_1} \right\rangle dw_1 + \text{c.c.} \quad (49)$$

This Berry phase does not give the braiding statistics expected for anyons because of the additional term. Moreover, this additional term contains nontrivial poles of w_1 that are functions of the lattice positions z_i . As a result, it depends on the size and shape of the contour c .

5.1.2. Isolating a Quasihole We explained above Equation (17), how taking the limit $w_2 \rightarrow \infty$ in Equation (16) leads to an isolated quasielectron at w_1 . One can similarly take the $w_1 \rightarrow \infty$ limit. In Equation (16), $\prod_{i=1}^N (w_1 - z_i)^{-n_i}$ becomes a z_i independent factor w_1^{-M} in that limit, which is absorbed in the normalization. Evidently this limit isolates the quasihole at w_2 .

We take the limit $w_1 \rightarrow \infty$ in Equation (46). We only need to investigate the behavior of $[1 - \mathcal{F}]$. Since w_1 is in the numerator of \mathcal{F} , we neglect the one in front. The problem is that this factor contains factors like $(z_l - z_k)^{q n_l n_k}$. Because of such dependence on z_1, \dots, z_N , we cannot absorb \mathcal{F} in the normalization.

6. Conclusion

In this paper, we studied the continuum limit of a lattice quasielectron ansatz. This lattice quasielectron, besides having the topological properties expected for an anyonic quasielectron, is the inverse of the lattice quasihole.

Our study reveals that a continuum limit of this lattice wavefunction does not exist. Only when the quasielectron is placed on top of a lattice site, this limit of the lattice quasielectron gives a finite result. Otherwise, depending on how we approach it, in the continuum limit the quasielectron pole gives rise to a slow $\ln N$ singularity, where N is the number of lattice sites. This also explains why such divergence is hard to observe in the numerics. We then try to salvage the ansatz wavefunction by projecting it on the LLL, which removes the singularity. We demonstrate that the projected state does not obtain the braiding properties expected for anyons. We hence conclude that taking the continuum limit of the lattice quasielectron wavefunction does not lead to a suitable ansatz for anyonic quasielectrons in the continuum.

Acknowledgments

We thank Maria Hermanns and Eddy Ardonne for several helpful discussions and comments on the manuscript.

References

- [1] D. C. Tsui, H. L. Stormer, and A. C. Gossard, Two-dimensional magnetotransport in the extreme quantum limit, *Phys. Rev. Lett.* **48**, 1559 (1982).
- [2] D. Tong, Lectures on the Quantum Hall Effect, [arXiv:1606.06687](https://arxiv.org/abs/1606.06687) (2016).
- [3] A. Stern, Anyons and the quantum Hall effect – A pedagogical review, *Ann. Phys.* **323**, 204 (2008).
- [4] J. K. Jain, *Composite Fermions* (Cambridge University Press, Cambridge, 2007).
- [5] A. Yu. Kitaev, Fault-tolerant quantum computation by anyons, *Ann. Phys.* **303**, 2 (2003).
- [6] R. B. Laughlin, Anomalous quantum Hall effect: An incompressible quantum fluid with fractionally charged excitations, *Phys. Rev. Lett.* **50**, 1395 (1983).
- [7] R. B. Laughlin, *Elementary theory: The incompressible quantum fluid*, in *The quantum Hall effect* (Springer, New York, 1987).

- [8] G. S. Jeon and J. K. Jain, Nature of quasiparticle excitations in the fractional quantum Hall effect, *Phys. Rev. B* **68**, 165346 (2003).
- [9] B. Yang and F. D. M. Haldane, Nature of quasielectrons and the continuum of neutral bulk excitations in Laughlin quantum Hall fluids, *Phys. Rev. Lett.* **112**, 026804 (2014).
- [10] G. S. Jeon, K. L. Graham, and J. K. Jain, Nature of quasiparticle excitations in the fractional quantum Hall effect, *Phys. Rev. Lett.* **91**, 036801 (2003).
- [11] B. A. Bernevig and F. D. M. Haldane, Clustering properties and model wave functions for non-Abelian fractional quantum Hall quasielectrons, *Phys. Rev. Lett.* **102**, 066802 (2009).
- [12] T. H. Hansson, C.-C. Chang, J. K. Jain, and S. Viefers, Composite-fermion wave functions as correlators in conformal field theory, *Phys. Rev. B* **76**, 075347 (2007).
- [13] T. H. Hansson, M. Hermanns, and S. Viefers, Quantum Hall quasielectron in conformal field theory, *Phys. Rev. B* **80**, 165330 (2009).
- [14] T. H. Hansson, M. Hermanns, N. Regnault, and S. Viefers, Conformal field theory approach to Abelian and non-Abelian quantum Hall quasielectrons, *Phys. Rev. Lett.* **102**, 166805 (2009).
- [15] J. Suorsa, S. Viefers, and T. H. Hansson, A general approach to quantum Hall hierarchies, *New Journal of Physics* **13**, 075006 (2011).
- [16] M. Greiter, V. Schnells, and R. Thomale, Laughlin states and their quasiparticle excitations on the torus, *Phys. Rev. B* **93**, 245156 (2016).
- [17] J. Kjäll, E. Ardonne, V Dwivedi, M. Hermanns, and T. H. Hansson, Matrix product state representation of quasielectron wave functions, *J. Stat. Mech.* **2018**, 053101 (2018).
- [18] A. E. B. Nielsen, I. Glasser, and I. D. Rodríguez, Quasielectrons as inverse quasiholes in lattice fractional quantum Hall models, *New J. Phys.* **20**, 033029 (2018).
- [19] T. Neupert, L. Santos, C. Chamon, and C. Mudry, Fractional quantum Hall states at zero magnetic field, *Phys. Rev. Lett.* **106**, 236804 (2011).
- [20] N. Regnault and B. Andrei Bernevig, Fractional Chern insulator, *Phys. Rev. X* **1**, 021014 (2011).
- [21] E. J. Bergholtz and Z. Liu, Topological flat band models and fractional Chern insulators, *Int. J. Mod. Phys. B* **27**, 1330017 (2013).
- [22] H.-H. Tu, A. E. B. Nielsen, J. I. Cirac, and G. Sierra, Lattice Laughlin states of bosons and fermions at filling fractions $1/q$, *New J. Phys.* **16**, 033025 (2014).
- [23] A. S. Sørensen, E. Demler, and M. D. Lukin, Fractional Quantum Hall States of Atoms in Optical Lattices, *Phys. Rev. Lett.* **94**, 086803 (2005).
- [24] M. Hafezi, A. S. Sørensen, E. Demler, and M. D. Lukin, Fractional quantum Hall effect in optical lattices, *Phys. Rev. A* **76**, 023613 (2007).
- [25] A. E. B. Nielsen, Anyon braiding in semianalytical fractional quantum Hall lattice models, *Phys. Rev. B* **91**, 041106(R) (2015).
- [26] I. D. Rodríguez and A. E. B. Nielsen, Continuum limit of lattice models with Laughlin-like ground states containing quasiholes, *Phys. Rev. B* **92**, 125105 (2015).
- [27] M. Abramowitz and I Stegun, *Handbook of mathematical functions with formulas, graphs, and mathematical tables* (United States Department of Commerce, National Bureau of Standards (NBS), 1964).